small
NANO MICRO
www.small-journal.com

Dual-Graphene Rechargeable Sodium Battery

Faxing Wang, Zaichun Liu, Panpan Zhang, Hongyan Li, Wenbo Sheng, Tao Zhang, Rainer Jordan, Yuping Wu, Xiaodong Zhuang, and Xinliang Feng**

Sodium (Na) ion batteries are attracting increasing attention for use in various electrical applications. However, the electrochemical behaviors, particularly the working voltages, of Na ion batteries are substantially lower than those of lithium (Li) ion batteries. Worse, the state-of-the-art Na ion battery cannot meet the demand of miniaturized in modern electronics. Here, we demonstrate that electrochemically exfoliated graphene (EG) nanosheets can reversibly store (PF_6^-) anions, yielding high charging and discharging voltages of 4.7 and 4.3 V vs. Na^+/Na, respectively. The dual-graphene rechargeable Na battery fabricated using EG as both the positive and negative electrodes provided the highest operating voltage among all Na ion full cells reported to date, together with a maximum energy density of 250 Wh kg^{-1}. Notably, the dual-graphene rechargeable Na microbattery exhibited an areal capacity of 35 µAh cm^{-2} with stable cycling behavior. This study offers an efficient option for the development of novel rechargeable microbatteries with ultra-high operating voltage and high energy density.

Energy storage has been a persistent global concern over the past decade, because of the urgent need to utilize renewable energy to solve the energy crisis and decrease environmental pollution. Li ion batteries have become one of the most crucial energy storage devices, particularly for portable electronic products and electric vehicles (EVs).[1] To achieve the sufficient voltage and energy to power an EV, hundreds to thousands of Li ion batteries must be connected in series/parallel to form a large-scale battery module. However, the enormous exploitation of Li resources driven by the ever-growing demand of EVs and large grids will eventually lead to the depletion because Li reserves are limited. Therefore, the increasing cost of lithium and its long-term availability concerns have triggered increasing interest in alternative rechargeable batteries.[2,3]

Na ion batteries have captured the scientific community's attention in recent years because, compared with Li, Na is one of the most abundant elements in the Earth's crust.[4] Currently, Na ion batteries are considered one of the most promising candidates for next-generation energy storage devices, which have high application potential in portable electronics, EVs, and smart grids. Various positive electrodes for Na ion batteries have been extensively investigated in the last several years.[5–14] However, these transition metal-containing positive electrodes display relatively low operating voltages in Na ion batteries. Specifically, with the exception of $Na_4V_2(PO_4)_2F_3$ and $Na_4Co_3(PO_4)P_2O_7$, which can provide working voltages of up to 4.0 V versus Na^+/Na, other positive electrodes show an average working voltage of only approximately 3.6 V versus Na^+/Na or less.[4] When these positive electrodes are assembled into Na ion full batteries using conventional negative electrodes (e.g., hard carbon), their operating voltages would be even lower (less than 3.3 V). Unfortunately, the low operating voltage usually leads to low energy density. Thus, the development of a Na-based battery system with a high operating voltage comparable to that of a commercial Li ion battery should be essential for the practical application. Interestingly, to improve the working voltage, anion intercalation into graphite was demonstrated in dual ion batteries, which displayed high voltage up to 5 V.[15–30] However, all the reported dual ion batteries were based on traditional rigid configuration,[15–30] which failed to provide in-plane thin film devices for practical application, especially for on-chip microelectronics.

In this study, we demonstrate a dual-graphene rechargeable Na battery realized by using electrochemically exfoliated graphene (EG) as both negative and positive electrodes. The positive electrode provides a high charge/discharge voltages of 4.7/4.3 V versus Na^+/Na, with capacities ranging from 90 to 120 mAh g^{-1}. The reversible electrochemical intercalation of PF_6^- into EG was confirmed through kinetic analysis, in situ Raman spectroscopy, ex situ X-ray diffraction (XRD) and ab initio calculation. The fabricated dual-graphene rechargeable

F. Wang, P. Zhang, H. Li, Dr. T. Zhang,
Dr. X. Zhuang, Prof. X. Feng
Center for Advancing Electronics Dresden (cfaed) & Department of Chemistry and Food Chemistry
Technische Universität Dresden
01062, Dresden, Germany
E-mail: xiaodong.zhuang@tu-dresden.de;
xinliang.feng@tu-dresden.de

Z. Liu, Prof. Y. Wu
School of Energy Science and Engineering
Nanjing Tech University
211816 Nanjing, China

W. Sheng, Prof. R. Jordan
Chair of Macromolecular Chemistry
School of Science
Technische Universität Dresden
01069 Dresden, Germany

The ORCID identification number(s) for the author(s) of this article can be found under https://doi.org/10.1002/smll.201702449.

DOI: 10.1002/smll.201702449

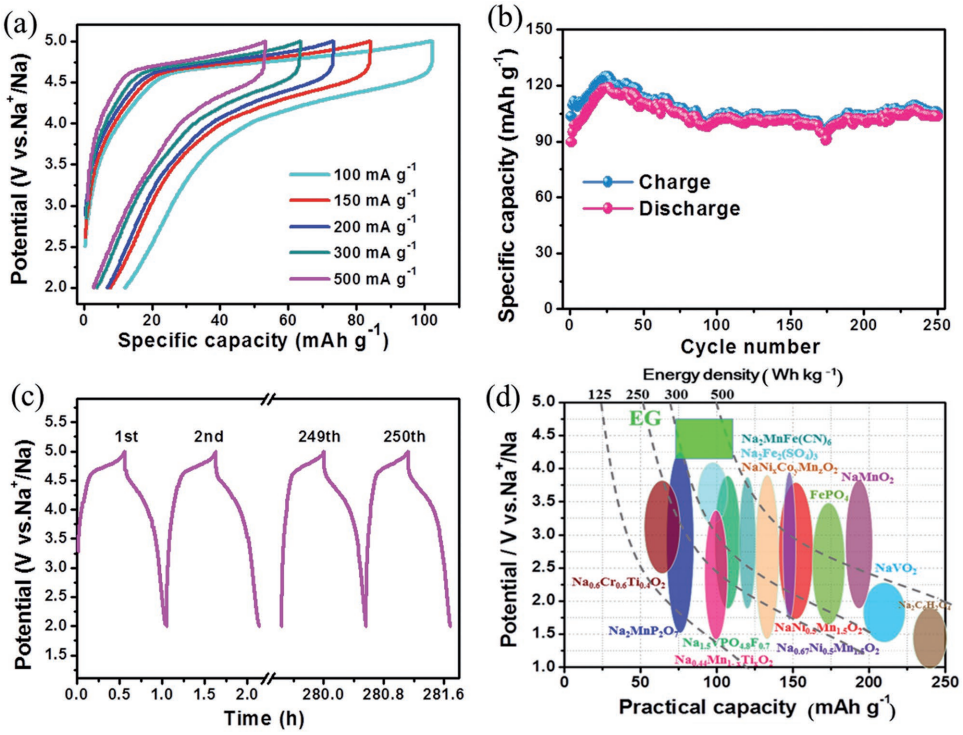

Figure 1. Electrochemical behavior of the positive electrode in the half cell. a) Galvanostatic charge/discharge profiles at various current densities. b) Cyclic performance at 100 mA g^{-1}. c) First, second, 249th, and 250th discharge/charge profiles at 100 mA g^{-1}. d) Plot summarizing the potential and energy density versus gravimetric capacity of the state-of-the-art positive electrodes for Na ion storage, together with anion storage in the positive electrode in this study.

Na battery delivers a maximal energy density (250 Wh kg^{-1}), excellent cycling stability with capacity retention of 95% after 200 cycles, and an ultrahigh operating voltage up to 4.0 V. Importantly, the dual-graphene rechargeable Na microbattery is demonstrated through spray-coating technology using EG ink, which exhibits a maximum areal capacity of 35 μAh cm^{-2} at 0.03 mA cm^{-2} with stable cycling behavior.

Different from the working mechanism of a conventional Na ion battery (Figure S1a, Supporting Information), the dual-graphene rechargeable Na battery fabricated in this work operates through cation (Na^+) and anion (PF_6^-) reversible intercalation reactions at the negative and positive electrodes, respectively (Figure S1b, Supporting Information). The used EG was prepared through a modified electrochemical exfoliation method (Figure S2a, Supporting Information) facilitating the gram-scale preparation of graphene.[31] Scanning electron microscopy (SEM) and transmission electron microscopy (TEM) showed the lateral feature of EG consisting of 4–6 layers (Figure S2b–e, Supporting Information). The intensity ratio of the D and G bands (I_D/I_G) of the EG sheets was ≈0.25, thus indicating substantially fewer defects in the EG (Figure S2f, Supporting Information). The reversible Na ion intercalation into graphite has been demonstrated using the solvent cointercalation in an ether-based electrolyte.[32–35] Similarly to that of graphite, an average intercalation potential was observed at 0.6 Vversus Na^+/Na for EG (Figure S3a, Supporting Information). The charge/discharge profiles demonstrated discharge and charge capacities of 131 and 120 mAh g^{-1} at 100 mA g^{-1}, respectively (Figure S3b, Supporting Information). The initial irreversible capacity of EG is attributed to the formation of a solid–electrolyte interphase layer.[4] The specific capacity was stable up to 250 cycles, with Coulombic efficiencies of nearly 100% (Figure S4, Supporting Information) at 100 mA g^{-1}.

EG exhibited high charge/discharge voltages of up to 4.7/4.3 V versus Na^+/Na in a half cell (**Figure 1**a). At the current density of 100 mA g^{-1}, an initial discharge capacity of 90 mAh g^{-1} was achieved. When the current density increased to 500 mA g^{-1}, its discharge capacity decreased to 52 mAh g^{-1}. Despite a relatively lower capacity compared with that of the positive electrodes containing transition metals in Na ion batteries,[4] the achieved capacity was still higher than those of $Na_2MnP_2O_7$ (80 mAh g^{-1} at 0.2 C),[36] $Na_{0.6}Cr_{0.6}Ti_{0.4}O_2$ (74 mAh g^{-1} at 0.1 C),[37] and $Na_{3.32}Fe_{2.34}(P_2O_7)_2$ (85 mAh g^{-1} at 0.05 C).[38] Figure 1b presents the charge/discharge cycling behavior of EG as the positive electrode. The discharge capacity was 90 mAh g^{-1} at the initial cycle. Then, it markedly increased to the maximum value of 120 mAh g^{-1} after 30 cycles. This capacity increase in the initial cycles may be attributed to the gradual electrolyte wetting process in the EG electrode.[19] Nevertheless, the capacity was maintained at more than 90 mAh g^{-1} after 250 cycles. No obvious polarization increase was observed in the voltage profiles after 250 cycles (Figure 1c). The Coulombic efficiency was 86% in the first cycle and then stabilized at 99% (Figure S5, Supporting Information). Notably, the working voltage (4.2–4.5 V versus Na^+/Na) of the half-cell was higher than those obtained for most reported metal-containing intercalation compounds as positive electrodes for Na ion batteries in the voltage range of 2–4 V versus Na^+/Na (Figure 1d).

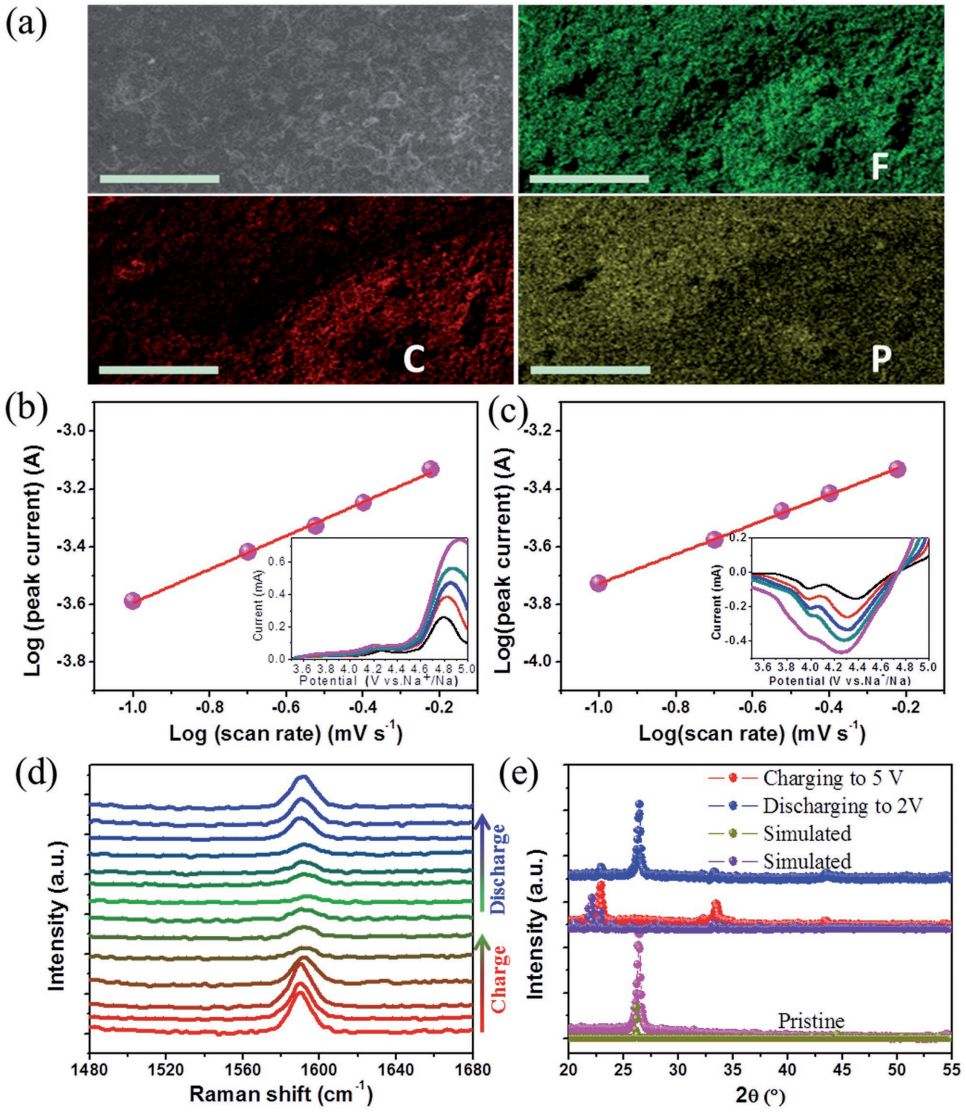

Figure 2. Anion diffusion mechanism at the positive electrode. a) SEM elemental mappings for the positive electrode after charging process. Scale bars, 500 nm. b,c) Kinetic analysis of the electrochemical behavior between the positive electrode and anions. Insets depict the corresponding current versus voltage curves. d) In situ Raman spectra recorded for the positive electrode through a charge/discharge cycle. e) Ex situ X-ray diffraction patterns of the positive electrode in the charging and discharging states in the half cell.

To investigate the mechanism of the reaction between the positive electrode and ions in the electrolyte, the half-cell was disassembled in a glove box after being charged to 5 V versus Na^+/Na, and the surface morphology of the positive electrode was characterized by SEM elemental mappings (**Figure 2**a). The F and P elements were distributed uniformly within the positive electrode surface. The F element should arise from the electrolyte (PF_6^-) or the binder (polyvinylidene difluoride (PVDF)), whereas the P element arises from the electrolyte (PF_6^-). To determine whether intercalation/deintercalation or adsorption/desorption of PF_6^- occurred, we plotted the log (i) versus log (v) for the oxidation/reduction peaks in the half cell. Theoretically, the peak currents (i) change with the sweep rate (v) and can be generally expressed as $i = av^b$, where a and b are constants.[39] The reaction is a surface-limited process if the b value is 1. While a redox reaction limited by semi-infinite diffusion means the b value is 0.5.[40] For sweep rates ranging from 0.1 to 0.6 mV s^{-1}, the b values for the anodic (Figure 2b) and cathodic (Figure 2c) processes were ≈0.52 and 0.58, respectively, as calculated from the slope values. This result indicates that the kinetics between PF_6^- and graphene nanosheets can be most accurately described as a redox reaction limited by semi-infinite diffusion; that is, the intercalation/deintercalation of the electrolyte anions into the EG layers is responsible for the electrochemical process.

In situ Raman spectroscopy was performed to probe the anion intercalation/deintercalation into/from graphene nanosheets during the charge/discharge process (Figure 2d). For the pristine positive electrode a relatively sharp peak at approximately 1580 cm^{-1} (G band) can be observed. With increasing charging time, the G band signal became broader and splits into a doublet (Figure S6a, Supporting

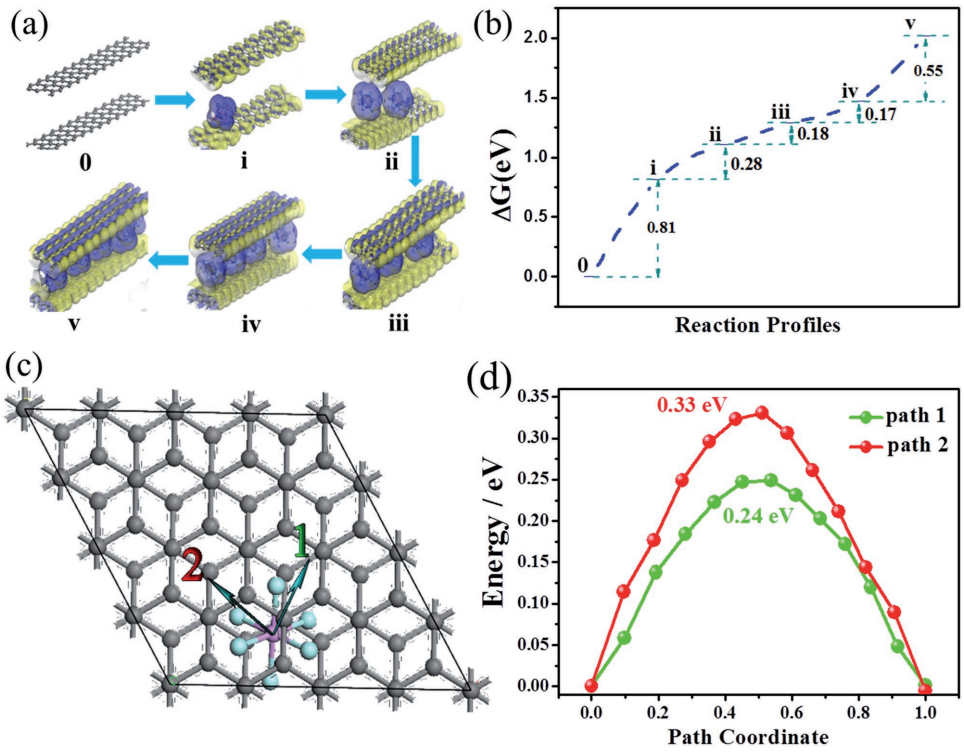

Figure 3. Theoretical calculation. a) Ab initio calculation for the reaction profiles of anion transport across the graphene layers and b) their energies at each step. Ab initio calculation on anion migration paths between graphene layers. c) Initial configuration and two diffusion paths for anion. d) Diffusion barriers calculated for the paths shown in panel (c).

Information), indicating the presence of two graphene populations, probably intercalant layers and the uncharged graphene layers. At the end of the charging process, the intensity of the blue-shifted G peak drastically decreases. The spectral changes were then reversed in the discharging process. This phenomenon is similar to that reported for the $AlCl_4^-$ intercalation/deintercalation into graphite in Al ion batteries.[41] Figure 2e presents the ex situ XRD patterns of the EG. The (002) peak originating from graphitic carbon suggests a low disorder degree of the EG.[42] In contrast to exfoliated graphite by a rapid thermal treatment under nitrogen atmosphere,[43] the EG exhibits a weak intensity of (002) peak as presented in Figure S6b in the Supporting Information, suggesting that the stacking interaction of EG is less pronounced than that in graphite and exfoliated graphite with thick flakes. The (002) peak of EG at 26.8° disappeared, whereas two new peaks emerged at 23° and 34° during charging to 5 V versus Na^+/Na, thus indicating the formation of anion intercalation compounds. Full discharging led to the recovery of the graphene peak, but the two peaks at 23° and 34° were maintained with decreased intensities. This result was probably caused by the irreversible changes in the interlayers between the graphene or the trapping of a small amount of PF_6^- species. In fact, not all the anions inserted into graphene could be extracted, as deduced from the Coulombic efficiency reaching just 86% during the first cycle.

To further understand the anion intercalation mechanism, the results of ab initio calculation based on density functional theory are presented in **Figure 3**. After the intercalation of several anions from i to iv (Figure 3a), $C_{72}(PF_6)_4$ (unit cell expansion from $C_{18}PF_6$) exhibits continuous isosurface contact areas between PF_6 and the graphene layers across the cross-section perpendicular to the graphene layers. A large contact area between the anion and graphene layers suggests a substantial electron transfer between them. As shown in Figure 3b, the energy barrier of the initial anion intercalation is the highest (0.81 eV), thus suggesting that the first PF_6^- must overcome higher energy barriers in order to intercalate into the graphene layers. For the second, third, and fourth anion intercalations, the energy barriers are 0.28, 0.18, and 0.17 eV, respectively. These calculated values indicate that the first anion intercalation can lower the energy barriers, thereby enabling the following anions to intercalate more easily. The next three anions follow the same rules after the first anion intercalation. Until the fifth anion intercalation, the energy barrier suddenly becomes large above 0.5 eV, indicating that the interspace for anion storage reaches the upper limit. This calculated result is consistent with the experimental result from the cyclic voltammetry curves (inset, Figure 2b). The current for the first oxidation peak at 4.3 V versus Na^+/Na was weak, whereas the second oxidation peak at 4.75 Vversus Na^+/Na was strong. The calculated result also suggests an "activation" process during the charge/discharge cycles, in which the initial anions (PF_6^-) are required to widen the graphene interlayer gaps at the electrode/electrolyte interface to promote the subsequent anion intercalation.[17,18] This process may also explain the gradual increase in the capacity during the early 30 cycles accompanying the increase in the electrochemical cycles (Figure 1b). In general, ion

diffusion in a few-layered graphene always involves two paths: parallel to the direction of the graphene surface[44] and perpendicular to the graphene surface.[45] Along (001) direction, that is perpendicular to the graphene surface, ion diffusion has a high energy barrier of 10.2 eV, suggesting that ion penetrating through the graphene plane is extremely difficult.[45] Thus, the paths in a direction parallel to the graphene surface are considered and shown in Figure 3c. Along the path one ((110) direction), anion only needs to pass a C–C bond to reach the next stable point. Differently, along the path two ((100) direction), anion needs to cross a C atom and then reach to stabilize after relaxation, which requires a higher barrier. Specifically, the barrier height along path one is 0.24 eV (Figure 3d), which is a little lower compared with Li diffusion in graphite in the range of 0.3–0.4 eV,[46] but higher than that of $AlCl_4$ diffusion in graphite (below 0.1 eV) in Al ion battery.[47] Normally, the low diffusion barrier indicates the high discharge rate. From experimental result, the rate capability of PF_6^- intercalation/deintercalation into graphene layers is better than that of Li^+ intercalation/deintercalation into graphene layers in Li ion battery,[48] but worse than that of $AlCl_4^-$ intercalation/deintercalation into graphene layers in Al ion battery.[41]

A dual-graphene rechargeable Na battery was then fabricated using EG as both the negative and positive electrodes. The discharge behaviour was first characterized by the polarization curve recorded ranging from 70 to 750 mA g^{-1}. The average discharge voltage reached up to 4 V at the low current densities (**Figure 4**a). At 300 and 400 mA g^{-1}, obvious decreases of the discharge voltages were observed because of the simultaneously increasing overpotential at the large current density. The large overpotential resulted from the gradually increasing polarization of the electrode redox reaction when increased the current density. The large polarization, as indicated by the increasing separation between reduction and oxidation processes, caused the decrease of the discharge voltage and increase of the charge voltage as shown in Figure 4a. At the current density of 300 mA g^{-1}, the full cell was operated with a power density of approximately 980 W kg^{-1} and a discharge voltage of 3.5 V. The operating voltage is higher than those of most Na ion batteries (Table S1, Supporting Information). The peak power output was approximately 1200 W kg^{-1} (Figure 4b). At 50 mA g^{-1}, the full cell produced a working voltage ranging from 3.5 to 4.0 V with a capacity of 68 mA h g^{-1} (Figure 4c). The energy densities of the dual-graphene rechargeable Na battery were calculated as 250, 190, and 145 Wh kg^{-1} at 50, 150, and 200 mA g^{-1}, respectively. Although the specific capacity of our full cell was not superior to those of some electrode materials containing transition metals, the excellent operating voltage made its energy density close to or even higher than those of state-of-the-art Na ion full cells, including $Na_2C_8H_2O_6//Na_4C_8H_2O_6$ (65 Wh kg^{-1}) and $Na_{0.6}[Cr_{0.6}Ti_{0.4}]O_2//Na_{0.6}[Cr_{0.6}Ti_{0.4}]O_2$ (94 Wh kg^{-1}).[13,37] Moreover, the full cell demonstrated excellent cycle stability, with capacity retention of 95% after 200 cycles (Figure 4d).

A simple demonstration for lighting commercial light-emitting diodes (LEDs) is presented to show a possible practical application of the dual-graphene rechargeable Na battery. One white LED (3.6 V; Figure S7a, Supporting Information) and two red LEDs connected in series (4 V; Figure S7b, Supporting Information) were lit for more than half an hour with a single dual-graphene rechargeable Na battery charged to 4.5 V. Moreover, the fast-growing popularity of microelectronics requires the continuous development of miniaturized power sources.

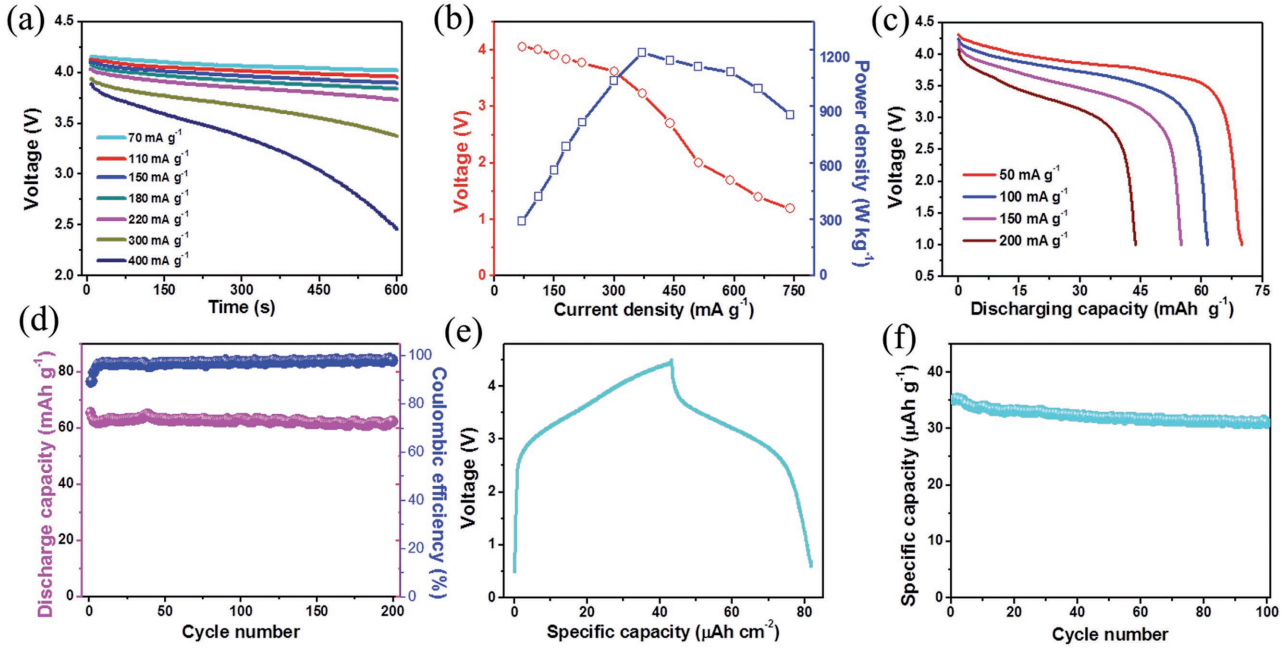

Figure 4. Electrochemical behavior of the dual-graphene rechargeable sodium battery and the microbattery. a) Discharge curves with a cutoff time of 10 min at various current densities. b) Polarization graph presenting discharge voltage and corresponding power density. c) Full discharge curves at various current densities. The specific capacities and energy densities are based on the total mass of the positive and negative electrodes. d) Cycling performance and Coulombic efficiency at 50 mA g^{-1} for 200 cycles. e) Charge/discharge curve and f) cycling behavior of the dual-graphene rechargeable Na microbattery.

Because the same material (graphene) is utilized for both positive and negative electrodes, the dual-graphene rechargeable Na microbattery could be easily realized through micropatterning or spray-coating technology.[49,50] For fabricating an in-plane microdevice, EG ink with 5% PVDF binder in isopropanol was spray-coated onto the separator (Celgard membrane) substrates and covered using a shadow mask (both finger and channel widths were 500 μm, and the length was 2 cm) (Figure S8, Supporting Information). Subsequently, the electrolyte was poured on the Celgard separator. The device was then sealed by the PET substrates. In contrast to the photolithographic and micromachining processes, the spray-coating technology is rapid and provides tunable electrode thickness by changing the time and concentration of the graphene ink. The single microbattery exhibited a maximum areal capacity of 35 μAh cm^{-2} at 0.3 mA cm^{-2} (Figure 4e), a value comparable to those of $LiCoO_2$ based thin-film Li ion batteries (12–40 μAh cm^{-2}).[49] Notably, the microdual-graphene rechargeable Na battery showed only 15% capacity decay after 100 cycles (Figure 4f), close to the capacity decay of thin-film Li ion batteries.[51,52]

Almost all previously reported Na ion batteries were based on transition-metal-containing electrode materials, which are environmentally unfriendly and high-cost, e.g., Sn, Ni, Co, etc.[53] Therefore, besides high operating voltage and in-plane microdevice, another advantage of dual-graphene rechargeable Na battery is that metal-containing electrodes are no longer needed. For the dual-graphene rechargeable Na battery, the electrochemically exfoliated graphene in both positive and negative electrodes is environment-friendly, transition-metal-free, and can be fabricated in large quantity. In addition, the choice of positive and negative electrode materials for our full cell is flexible. In the case of positive electrodes, the concept of the reversible anion intercalation can be extended to the use of other graphitic carbon, such as carbon nanotubes (CNTs) and hollow graphitized carbon nanospheres (Figures S9–S12, Supporting Information). Redox peaks were observed when CNTs were used as the positive electrode. The specific capacities of CNT and hollow graphitized carbon nanospheres electrodes were slightly lower than that of EG. However, both CNT and hollow graphitized carbon nanospheres exhibited superior stable capacity retentions compared with that of EG. This was mainly due to the hollow interior structure that effectively alleviated the structural strain during the anion intercalation/deintercalation processes. For the negative electrodes, alternative materials, such as alloys, hard carbon, and metal sulfides,[20,21] with lower working voltages or high specific capacities could also be used to further improve the operating voltage or specific capacity of this type of rechargeable battery.

In summary, we presented a novel dual-graphene rechargeable Na microbattery with electrochemically exfoliated graphene as both the positive and negative electrodes. Because of the reversible anion (PF_6^-) intercalation/deintercalation into and out of the electrochemically exfoliated graphene at high charge/discharge voltages of 4.7 and 4.3 V versus Na^+/Na, respectively, the fabricated in-plane microbattery delivered high operating voltage up to 4.0 V. The high-voltage microbattery proposed in this study should offer new opportunities for designing green miniaturized energy storage devices without using complicated and toxic transition metal-containing electrodes.

Supporting Information

Supporting Information is available from the Wiley Online Library or from the author.

Acknowledgements

F.W. and Z.L. contributed equally to this work. This work was financially supported by the German Research Foundation (DFG) within the Cluster of Excellence "Center for Advancing Electronics Dresden" (cfaed), ERC Grant on 2DMATER, UP-GREEN and EU Graphene Flagship. Z.L. and Y.W. would like to express the financial support of National Natural Science Foundation Committee of China (Distinguished Youth Scientists Project of 51026004, and U1601214) and National Materials Genome Project (2016YFB0700600).

Conflict of Interest

The authors declare no conflict of interest.

Keywords

anion intercalation, electrochemically exfoliated graphene, high voltage, microbattery, rechargeable battery

Received: July 18, 2017
Revised: August 19, 2017
Published online: October 27, 2017

[1] C. Y. Wang, G. Zhang, S. Ge, T. Xu, Y. Ji, X. G. Yang, Y. Leng, *Nature* **2016**, *529*, 515.
[2] J. Sun, H. W. Lee, M. Pasta, H. Yuan, G. Zheng, Y. Sun, Y. Li, Y. Cui, *Nat. Nanotechnol.* **2015**, *10*, 980.
[3] D. Larcher, J. M. Tarascon, *Nat. Chem.* **2015**, *7*, 19.
[4] N. Yabuuchi, K. Kubota, M. Dahbi, S. Komaba, *Chem. Rev.* **2014**, *114*, 11636.
[5] N. Yabuuchi, M. Kajiyama, J. Iwatate, H. Nishikawa, S. Hitomi, R. Okuyama, R. Usui, Y. Yamada, S. Komaba, *Nat. Mater.* **2012**, *11*, 512.
[6] Y. U. Park, D. H. Seo, H. S. Kwon, B. Kim, J. Kim, H. Kim, I. Kim, H. I. Yoo, K. Kang, *J. Am. Chem. Soc.* **2013**, *135*, 13870.
[7] F. Wang, X. Wu, C. Li, Y. Zhu, L. Fu, Y. Wu, X. Liu, *Energy Environ. Sci.* **2016**, *9*, 3570.
[8] J. Billaud, R. J. Clement, A. R. Armstrong, J. Canales-Vazquez, P. Rozier, C. P. Grey, P. G. Bruce, *J. Am. Chem. Soc.* **2014**, *136*, 17243.
[9] Y. Sun, L. Zhao, H. Pan, X. Lu, L. Gu, Y. S. Hu, H. Li, M. Armand, Y. Ikuhara, L. Chen, X. Huang, *Nat. Commun.* **2013**, *4*, 1870.
[10] J. Song, L. Wang, Y. Lu, J. Liu, B. Guo, P. Xiao, J. J. Lee, X. Q. Yang, G. Henkelman, J. B. Goodenough, *J. Am. Chem. Soc.* **2015**, *137*, 2658.
[11] Y. Wang, J. Liu, B. Lee, R. Qiao, Z. Yang, S. Xu, X. Yu, L. Gu, Y. S. Hu, W. Yang, K. Kang, H. Li, X. Q. Yang, L. Chen, X. Huang, *Nat. Commun.* **2015**, *6*, 6401.
[12] J. Y. Hwang, S. M. Oh, S. T. Myung, K. Y. Chung, I. Belharouak, Y. K. Sun, *Nat. Commun.* **2015**, *6*, 6865.
[13] S. Wang, L. Wang, Z. Zhu, Z. Hu, Q. Zhao, J. Chen, *Angew. Chem., Int. Ed.* **2014**, *53*, 5892.
[14] B. Zhang, R. Dugas, G. Rousse, P. Rozier, A. M. Abakumov, J. M. Tarascon, *Nat. Commun.* **2016**, *7*, 10308.
[15] R. T. Carlin, H. C. De Long, J. Fuller, P. C. Trulove, *J. Electrochem. Soc.* **1994**, *141*, L73.

[16] J. A. Seela, J. R. Dahn, *J. Electrochem. Soc.* **2000**, *147*, 892.
[17] W. Marklea, N. Tran, D. Goers, M. E. Spahr, P. Novak, *Carbon* **2009**, *47*, 2727.
[18] T. Placke, S. Rothermel, O. Fromm, P. Meister, S. F. Lux, J. Huesker, H. W. Meyer, M. Winter, *J. Electrochem. Soc.* **2013**, *160*, A1979.
[19] J. A. Read, A. V. Cresce, M. H. Ervin, K. Xu, *Energy Environ. Sci.* **2014**, *7*, 617.
[20] S. Rothermel, P. Meister, G. Schmuelling, O. Fromm, H. W. Meyer, S. Nowak, M. Winter, T. Placke, *Energy Environ. Sci.* **2014**, *7*, 3412.
[21] S. Miyoshi, H. Nagano, T. Fukuda, T. Kurihara, M. Watanabe, S. Ida, T. Ishihara, *J. Electrochem. Soc.* **2016**, *163*, A1206.
[22] X. Zhang, Y. Tang, F. Zhang, C. S. Lee, *Adv. Energy Mater.* **2016**, *6*, 1502588.
[23] I. A. Rodríguez-Perez, Z. Jian, P. K. Waldenmaier, J. W. Palmisano, R. S. Chandrabose, X. Wang, M. M. Lerner, R. G. Carter, X. Ji, *ACS Energy Lett.* **2016**, *1*, 719.
[24] X. Tong, F. Zhang, B. Ji, M. Sheng, Y. Tang, *Adv. Mater.* **2016**, *28*, 9979.
[25] L. Fan, Q. Liu, S. Chen, K. Lin, Z. Xu, B. Lu, *Small* **2017**, *13*, 1701011.
[26] B. Ji, F. Zhang, N. Wu, Y. Tang, *Adv. Energy Mater.* **2017**, https://doi.org/10.1002/aenm.201700920.
[27] L. Fan, Q. Liu, S. Chen, Z. Xu, B. Lu, *Adv. Energy Mater.* **2017**, *7*, 1602778.
[28] M. Sheng, F. Zhang, B. Ji, X. Tong, Y. Tang, *Adv. Energy Mater.* **2017**, *7*, 1601963.
[29] C. Jiang, Y. Fang, J. Lang, Y. Tang, *Adv. Energy Mater.* **2017**, *29*, 1700519.
[30] B. Ji, F. Zhang, X. Song, Y. Tang, *Adv. Mater.* **2017**, https://doi.org/10.1002/adma.201700519.
[31] S. Yang, A. G. Ricciardulli, S. Liu, R. Dong, M. R. Lohe, A. Becker, M. A. Squillaci, P. Samorì, K. Müllen, *Angew. Chem., Int. Ed.* **2017**, *56*, 6669.
[32] B. Jache, P. Adelhelm, *Angew. Chem., Int. Ed.* **2014**, *53*, 10169.
[33] H. Kim, J. Hong, G. Yoon, H. Kim, K. Y. Park, M. S. Park, W. S. Yoon, K. Kang, *Energy Environ. Sci.* **2015**, *8*, 2963.
[34] Z. Zhu, F. Cheng, Z. Hu, Z. Niu, J. Chen, *J. Power Sources* **2015**, *293*, 626.
[35] H. Kim, J. Hong, Y. U. Park, J. Kim, I. Hwang, K. Kang, *Adv. Funct. Mater.* **2015**, *25*, 534.
[36] C. S. Park, H. Kim, R. A. Shakoor, E. Yang, S. Y. Lim, R. Kahraman, Y. Jung, J. W. Choi, *J. Am. Chem. Soc.* **2013**, *135*, 2787.
[37] Y. Wang, R. Xiao, Y. S. Hu, M. Avdeev, L. Chen, *Nat. Commun.* **2015**, *6*, 6954.
[38] K. H. Ha, S. H. Woo, D. Mok, N. S. Choi, Y. Park, S. M. Oh, Y. Kim, J. Kim, J. Lee, L. F. Nazar, K. T. Lee, *Adv. Energy Mater.* **2013**, *3*, 770.
[39] V. Augustyn, J. Come, M. A. Lowe, J. W. Kim, P. L. Taberna, S. H. Tolbert, H. D. Abruña, P. Simon, B. Dunn, *Nat. Mater.* **2013**, *13*, 518.
[40] X. Dong, L. Chen, J. Liu, S. Haller, Y. Wang, Y. Xia, *Sci. Adv.* **2016**, *2*, e1501038.
[41] M. C. Lin, M. Gong, B. Lu, Y. Wu, D. Y. Wang, M. Guan, M. Angell, C. Chen, J. Yang, B. J. Hwang, H. Dai, *Nature* **2015**, *520*, 325.
[42] J. Zhao, G. Zhou, K. Yan, J. Xie, Y. Li, L. Liao, Y. Jin, K. Liu, P. C. Hsu, J. Wang, H. M. Cheng, Y. Cui, *Nat. Nanotechnol.* **2017**, https://doi.org/10.1038/NNANO.2017.129.
[43] G. Cheng, I. Calizo, C. A. Hacker, C. A. Richter, A. R. H. Walker, *Carbon* **2016**, *96*, 311.
[44] L. J. Zhou, Z. F. Hou, L. M. Wu, Y. F. Zhang, *J. Phys. Chem. C* **2014**, *118*, 28055.
[45] F. Yao, F. Günes, H. Q. Ta, S. M. Lee, S. J. Chae, K. Y. Sheem, C. S. Cojocaru, S. S. Xie, Y. H. Lee, *J. Am. Chem. Soc.* **2012**, *134*, 8646.
[46] K. Persson, V. A. Sethuraman, L. J. Hardwick, Y. Hinuma, Y. S. Meng, A. van der Ven, V. Srinivasan, R. Kostecki, G. Ceder, *J. Phys. Chem. Lett.* **2010**, *1*, 1176.
[47] M. L. Agiorgousis, Y. Y. Sun, S. Zhang, *ACS Energy Lett.* **2017**, *2*, 689.
[48] J. Wang, J. Huang, R. Yan, F. Wang, W. Cheng, Q. Guo, J. Wang, *J. Mater. Chem. A* **2015**, *3*, 3144.
[49] Z. S. Wu, K. Parvez, X. Feng, K. Mullen, *Nat. Commun.* **2013**, *4*, 2478.
[50] Z. Liu, Z. S. Wu, S. Yang, R. Dong, X. Feng, K. Müllen, *Adv. Mater.* **2016**, *28*, 2217.
[51] M. E. Donders, W. M. Arnoldbik, H. C. M. Knoops, W. M. M. Kessels, P. H. L. Notten, *J. Electrochem. Soc.* **2013**, *160*, A3066.
[52] Y. Liu, M. Clark, Q. Zhang, D. Yu, D. Liu, J. Liu, G. Cao, *Adv. Energy Mater.* **2011**, *1*, 194.
[53] J. Y. Hwang, S. T. Myung, Y. K. Sun, *Chem. Soc. Rev.* **2017**, *46*, 3529.